JACS
JOURNAL OF THE AMERICAN CHEMICAL SOCIETY

Article

pubs.acs.org/JACS

Exploiting Localized Surface Binding Effects to Enhance the Catalytic Reactivity of Peptide-Capped Nanoparticles

Ryan Coppage,[1] Joseph M. Slocik,[2] Hadi Ramezani-Dakhel,[3] Nicholas M. Bedford,[2,1] Hendrik Heinz,[3] Rajesh R. Naik,[2,*] and Marc R. Knecht[1,*]

[1]Department of Chemistry, University of Miami, Coral Gables, Florida 33146, United States

[2]Materials and Manufacturing Directorate, Air Force Research Laboratory, Wright-Patterson Air Force Base, Ohio 45433-7702, United States

[3]Department of Polymer Engineering, University of Akron, Akron, Ohio, 44325, United States

Supporting Information

ABSTRACT: Peptide-based methods represent new approaches to selectively produce nanostructures with potentially important functionality. Unfortunately, biocombinatorial methods can only select peptides with target affinity and not for the properties of the final material. In this work, we present evidence to demonstrate that materials-directing peptides can be controllably modified to substantially enhance particle functionality without significantly altering nanostructural morphology. To this end, modification of selected residues to vary the site-specific binding strength and biological recognition can be employed to increase the catalytic efficiency of peptide-capped Pd nanoparticles. These results represent a step toward the *de novo* design of materials-directing peptides that control nanoparticle structure/function relationships.

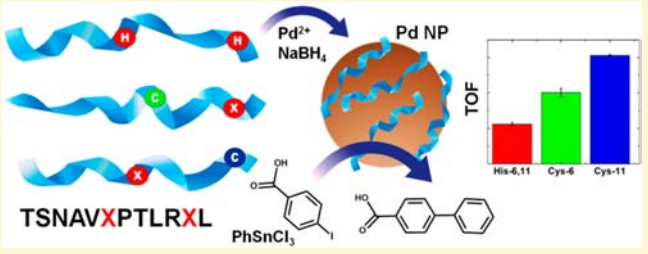

INTRODUCTION

Biology provides exquisite inspiration for the production of functional inorganic nanomaterials.[1] Most of these materials are prepared using peptides and proteins to direct structural growth and engender the system with desired properties.[1−3] Mimicking these approaches for the generation of technologically useful nanomaterials represents an avenue to achieve important structures for sustainable activities. Many groups have turned to biocombinatorial approaches to isolate peptides with affinity for a range of nonbiological materials;[1,4−7] however, the effect of the biotic/abiotic interface over the structure/function relationship remains poorly understood. To this end, the ability to fine-tune desirable optical, catalytic, magnetic, and other material properties could be achieved at the peptide sequence level.

We have employed the Pd-specific Pd4 peptide (TSNAVHPTLRHL) for the fabrication of peptide-capped Pd nanoparticles with the ability to catalyze C−C coupling reactions under nontraditional conditions of a water-based solvent at room temperature.[8,9] The peptide is anticipated to anchor to the metallic surface through the histidine residues at the six and eleven position,[10] where substitutions at these sites results in changes to the particle size and catalytic activity.[11,12] In this regard, we hypothesize that weaker binding at the six position, and stronger binding at the eleven position could result in peptides that produce nanoparticles with optimized catalytic functionality. Note that binding changes at these specific positions may alter the global peptide binding strength; however, the residue-specific binding effects are anticipated to be more important in controlling the surface bound peptide structure and the biotic/abiotic interface of the material, which likely participates in the reactivity.

In this work, we demonstrate that we can rationally modify materials binding peptide sequences to enhance the structure/function relationship of Pd nanoparticles for catalytic functionality; however, such approaches could be adapted for nanomaterials with other properties. To this end, the Pd4 peptide was employed as the parent sequence wherein the six and eleven positions were substituted with cysteine, histidine, and alanine residues. These amino acids were selected to modulate the binding strength at these specific positions with cysteine being the strongest binder, alanine the weakest, and the native histidine being of intermediate binding strength.[13] From this, six different peptides were generated, listed in Table 1, which were used to prepare peptide-capped Pd nanoparticles. Complete characterization of the peptide binding effects were studied using both experimental and modeling approaches, followed by their catalytic analysis using Stille C−C coupling. From these studies, the particles demonstrated reactivities that varied based solely upon the binding strength of the residues at the predetermined positions. Interestingly, no correlation between the global peptide binding strength and catalytic functionality was noted, supporting the hypothesis that

Received: March 2, 2013
Published: July 18, 2013

   dx.doi.org/10.1021/ja402215t | J. Am. Chem. Soc. 2013, 135, 11048−11054

Table 1. Pd4 and Cysteine Analogue Peptides

Peptide	Sequence	Size	TOF[a]
Pd4	TSNAVHPTLRHL	2.0 ± 0.4 nm	2234 ± 99
C6	TSNAVCPTLRHL	2.2 ± 0.3 nm	3963 ± 28
C11	TSNAVHPTLRCL	2.4 ± 0.4 nm	6138 ± 55
C6,11	TSNAVCPTLRCL	2.3 ± 0.4 nm	3974 ± 280
A6C11	TSNAVAPTLRCL	2.4 ± 0.4 nm	6097 ± 65
C6A11	TSNAVCPTLRAL	2.4 ± 0.4 nm	4147 ± 340

a = mol product (mol Pd × h)$^{-1}$

localized, residue-specific binding effects dominate property control, which was reinforced by theoretical modeling of the binding effects of the peptide on the Pd surface. Taken together, these results are important as they demonstrate that peptide design could be employed to generate sequences that optimize material properties, which cannot be selected for through biocombinatorial approaches.

EXPERIMENTAL SECTION

Chemicals. FMOC-protected Wang resins, functionalized with a protected leucine residue, FMOC-protected amino acids, diisopropyl ethylamine (DIPEA), piperidine, *N*-hydroxybenzotriazole (HoBT), and *O*-benzotriazole-*N*,*N*,*N*′,*N*′-tetramethyluronium hexafluorophosphate (HBTU) were purchased from Advanced Chemtech. Triisopropylsilane, 4-iodobenzoic acid, and K_2PdCl_4 were purchased from Sigma-Aldrich. $NaBH_4$, $CDCl_3$, phenyltin trichloride ($PhSnCl_3$), trifluoroacetic acid (TFA), anhydrous Na_2SO_4, NaCl, and KOH were acquired from VWR. *N*,*N*-dimethylformamide (DMF), acetonitrile, diethyl ether, and methanol were purchased from VWR. All chemicals were used as received. Synergy Ultrapure UV water (18mΩ•cm; Millipore) was used for all experiments.

Nanoparticle Synthesis. Peptides were synthesized via standard FMOC synthetic protocols,[14] purified by reverse-phase HPLC, and confirmed by MALDI-TOF mass spectrometry. Once the sequence was confirmed, the peptides were used to fabricate peptide-capped Pd nanoparticles at a 3.3:1 Pd:peptide ratio, as previously described.[9] Briefly, for each peptide, a 4.90 mL solution of ∼150 μM of each peptide and 500 μM K_2PdCl_4 were prepared as Pd^{2+}-peptide complex reactions. After the complexes were allowed to incubate for 30.0 min to ensure completion of the binding event, 100 μL of a freshly prepared 100 mM $NaBH_4$ solution was added, which resulted in nanoparticle formation. To complete the reduction process, the reaction was allowed to stand for 1.00 h.

Catalytic Analysis. For the catalytic analyses, the Stille C−C coupling reaction was employed.[9,12,15] For this reaction, 1.25 mmol of 4-iodobenzoic acid and 1.56 mmol of $PhSnCl_3$ were codissolved in sufficient 2.25 M KOH. After dissolution, 1.25 mL of the stock Pd nanoparticles was added, resulting in a 0.05 mol % Pd concentration. The final volume of the reaction was 20.0 mL, which was accounted for based upon the volume of KOH added. After reaction initiation, 2.0 mL aliquots were extracted and quenched with 12.5 mL of 5.0% HCl at selected time points over a 1.00 h reaction time. The final product, biphenylcarboxylic acid, was extracted and quantitated using described methods.[9]

Characterization. A 5.00 μL sample of each nanoparticle solution was deposited and allowed to dry on a 400-mesh Cu grid coated with an ultrathin carbon layer. TEM images were obtained with a JEOL 2010F or Phillips CM 200, operating at 200 kV, or an FEI Titan TEM operating at 300 kV. The analysis of at least 100 nanoparticles among multiple images was employed to determine particle size distributions. For Quartz Crystal Microbalance with dissipation energy (QCM-D) measurements, Pd surfaces were prepared by sputter-coating Pd onto Au QCM sensors for 180 s with a Cressington 108-Auto sputter coater. The metallic surfaces were then cleaned via UV/ozone exposure for 10.0 min, followed by a deionized water rinse, and an additional 10.0 min UV/ozone exposure. Each peptide was dissolved in water at concentrations of 2.5, 5.0, 7.5, 10.0, and 15.0 μg/mL. QCM measurements were obtained with a Q-Sense E4 QCM-D system, in which standard flow modules were employed. A flow rate of 0.15 mL/min was used for each analysis. The third overtone frequency was fit using a Langmuir isotherm from which the binding constants can be determined via known methods.[16] CD spectra were obtained on a Jasco J-815 CD spectrometer using a 750 μL quartz cuvette with a path length of 0.5 cm. Peptides were dissolved in water where a concentration of 16 μM was used for all measurements. Nanoparticles were prepared at equivalent ratios and likewise diluted for CD. The CDPro software package was used for analysis of CD spectra to deconvolute secondary structure contributions.

Molecular Simulation. Models of Pd {111} surfaces and the six peptides (Pd4, C6, C11, C6,11, C6A11, and A6C11) in aqueous solution were prepared on the scale of ∼3 × 3 × 6 nm^3. The models were subjected to molecular dynamics simulation using the INTERFACE-CHARMM force field (same as CHARMM-METAL force field), including extensions for partially covalent binding of Cys residues, as well as advanced equilibration and sampling techniques. Binding conformations, adsorption energies, and the role of specific residues to surface binding were analyzed as an average over more than 20 ns simulation time for each peptide (see details in the Supporting Information).

RESULTS AND DISCUSSION

Based on modeling studies, which predicted metal surface binding at the six and eleven positions of the native Pd4 peptide, a set of six different sequences was prepared (Table 1).[10] Pd4 possesses histidine residues at both locations. To site specifically increase the binding strength at these locations, two single cysteine modified peptides, C6 and C11, were prepared that substituted the histidine residue for cysteine at the six and eleven positions, respectively, while a double modification peptide, C6,11, was also generated that modified both histidines to cysteines. Two additional peptides were also designed that included both cysteine and alanine modifications: the A6C11 that incorporated an alanine at the sixth position and a cysteine at the eleventh position and the C6A11 peptide with a cysteine and alanine modification at the six and eleven positions, respectively. These two sequences were generated to substantially change the binding strength at the two positions, where minimal to no binding at the alanine sites was anticipated, with the strongest binding from the cysteine residues.

QCM analysis was initially employed to determine changes in the global Pd affinity of the peptides based upon the sequence changes. Figure 1a presents the observed frequency changes for the C6A11 peptide binding to a Pd sensor at five selected concentrations. As anticipated for all peptide concentrations, as time increases, the change in frequency decreases until saturation, consistent with binding of the target surface. Note that an inverted plot is presented to enhance the

dx.doi.org/10.1021/ja402215t | J. Am. Chem. Soc. 2013, 135, 11048−11054

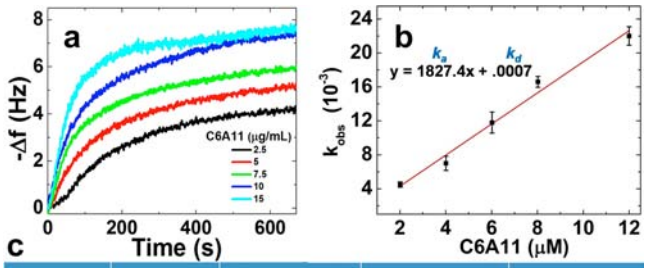

c

peptide	k_a ($M^{-1}s^{-1}$)	$k_d \times 10^{-3}$ (s^{-1})	$K_{eq} \times 10^5$ (M^{-1})	ΔG (kJ/mol)
Pd4	1693 ± 169	2.8 ± 0.6	6.1 ± 1.3	-33.0 ± 0.5
C6	1991 ± 117	1.0 ± 0.4	19.9 ± 7.3	-35.9 ± 0.9
C11	1474 ± 132	1.0 ± 0.5	14.7 ± 7.4	-35.1 ± 1.2
C6,11	1722 ± 72	1.0 ± 0.5	17.2 ± 8.5	-35.5 ± 1.2
A6C11	1563 ± 210	2.8 ± 0.9	5.6 ± 1.9	-32.7 ± 0.8
C6A11	1827 ± 113	0.7 ± 0.4	26.1 ± 14.2	-36.5 ± 1.3

Figure 1. QCM analysis of peptide binding: (a) observed frequency changes based upon peptide binding as a function of C6A11 concentration, (b) plot of the calculated k_{obs} values as a function of C6A11 concentration, and (c) Pd adsorption analysis for the parent Pd4 peptide and cysteine analogues.

clarity of data presentation. From the raw QCM data, a series of five k_{obs} values were determined employing previously described methods,[16] which were then plotted against the peptide concentration (Figure 1b). Linear fitting of the data was then used to determine the association (k_a) and dissociation (k_d) constants of peptide binding from the slope and *y*-intercept values of the best-fit line, respectively.[16] Similar studies were conducted for all of the peptides of Table 1 (Supporting Information, Figure S1), where the binding constants for all sequences are listed in Figure 1c. From this analysis, the parent Pd4 peptide was observed to possess a k_a of 1693 ± 169 M^{-1} s^{-1} and a k_d of 0.0028 ± 0.0006 s^{-1}, which results in a K_{eq} value of 6.1 × 10^5 ± 1.3 × 10^5 M^{-1} and a ΔG value of −33.0 ± 0.5 kJ/mol. Interestingly, when cysteine-only modifications were employed (C6, C11, and C6,11), while slightly lower k_a values were noted compared to the Pd4, substantially diminished k_d values were observed. As a result, significantly increased K_{eq} values of 1.99 × 10^6 ± 7.3 × 10^5 M^{-1}, 1.47 × 10^6 ± 7.4 × 10^5 M^{-1}, and 1.72 × 10^6 ± 8.5 × 10^5 M^{-1} were determined for the C6, C11, and C6,11 peptides, respectively. This in turn leads to more negative ΔG values of −35.9 ± 0.9 kJ/mol for the C6, −35.1 ± 1.2 kJ/mol for the C11, and −35.5 ± 1.2 kJ/mol for the C6,11 peptides, indicating a greater affinity for Pd.

When both alanine and cysteine-based peptide modifications were employed, unique changes in the Pd binding constants were observed. For instance, analysis of the A6C11 peptide demonstrated k_a and k_d values of 1563 ± 210 M^{-1} s^{-1} and 0.0028 ± 0.0009 s^{-1}, respectively, thus resulting in a K_{eq} of 5.6 × 10^5 ± 1.9 × 10^5 M^{-1} and a ΔG of −32.7 ± 0.8 kJ/mol. Such values are quite similar to those observed for the parent Pd4 peptide, suggesting that the increased binding effect of the cysteine residue may be offset by the weakened binding of the alanine. Analysis of the C6A11, however, demonstrated binding constants of 1827 ± 113 M^{-1} s^{-1}, 0.0007 ± 0.0004 s^{-1}, 2.61 × 10^6 ± 1.42 × 10^6 M^{-1}, and −36.5 ± 1.3 kJ/mol for the k_a, k_d, K_{eq}, and ΔG values, respectively. From this analysis, the strongest binding was observed from the C6A11 peptide, within the error of the analysis, while the weakest binding was observed from the A6C11. Such results were somewhat surprising as alanine modifications were anticipated to diminish the binding strength regardless of the position; however, changes to the peptide sequence/conformation may occur to increase the affinity. Indeed, based upon computational modeling discussed later, when bound to a Pd surface, increased peptide flexibility was noted for the A6C11 peptide as compared to the C6A11 sequence, consistent with their degrees of surface affinity. Furthermore, altered biotic/abiotic interfaces are likely, which were confirmed via CD analysis of the peptides before and after nanoparticle binding (discussed below).

Upon confirmation of the Pd affinity, the peptides were employed as passivating ligands to fabricate Pd nanoparticles using standard approaches.[8,9] The materials were then analyzed *via* UV−vis spectroscopy and transmission electron microscopy (TEM). UV−vis analysis of each peptide solution displayed a relatively featureless spectrum as anticipated (Supporting Information, Figure S2). Upon addition of K_2PdCl_4, the spectra of the Pd^{2+} complexed peptides demonstrated the appearance of a ligand-to-metal charge transfer (LMCT) band at ∼215 nm. After addition of $NaBH_4$, the reduced materials displayed a broad absorbance that increased toward lower wavelengths and the lack of an LMCT peak, all of which suggested nanoparticle formation.[8,9]

TEM imaging of the materials capped with the designed peptides is presented in Figure 2. For the Pd4-capped particles,

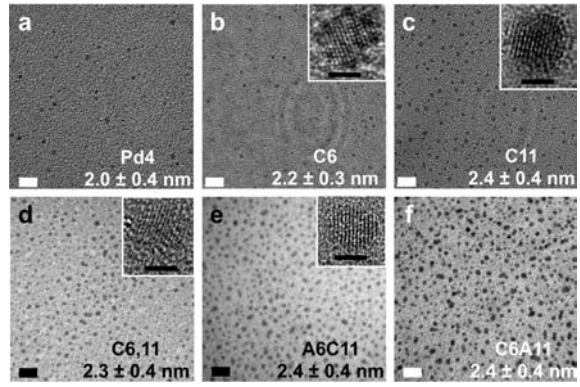

Figure 2. TEM analysis of the Pd nanoparticles capped with (a) Pd4, (b) C6, (c) C11, (d) C6,11, (e) A6C11, and (f) C6A11. Main scale bars are 10 nm, while inset bars are 2 nm.

an average size of 2.0 ± 0.4 nm was noted, consistent with previous studies;[8] however, for the particles prepared with the cysteine-substituted peptides, a slight size increase to 2.2 ± 0.3 nm (C6), 2.4 ± 0.4 nm (C11), and 2.3 ± 0.4 nm (C6,11) was observed. Furthermore, for the materials capped with either the A6C11 or C6A11 peptide, particles of an identical size and distribution of 2.4 ± 0.4 nm were noted. High-resolution analysis of selected cysteine-containing materials, shown as inserts in Figure 2, demonstrated the formation of single crystal particles; Pd4-based systems have been shown to produce single crystals particles.[8,11] Such similar sizes for the particles prepared with the A6C11 and C6A11 peptides were surprising as they have different binding affinities, based upon their ΔG values; however, such results may be related to the interaction mechanism of individual residues with the surface rather than the aggregate metallic affinity of the peptide.[12,17] This suggests that the resultant particle size is based upon factors such as peptide binding motifs and surface recognition elements, rather than on the absolute degree of affinity for the target material. It

dx.doi.org/10.1021/ja402215t | J. Am. Chem. Soc. 2013, 135, 11048−11054

is also interesting to note that particles of nearly the same size were generated with the designed sequences (2.2 − 2.4 nm). Such results are different than previous work with alanine-only substituted peptides that displayed controllable changes in particle size based upon sequence modifications.[11] This indicates that the presence of cysteine residues may modify the biorecognition capabilities of the peptides through metal−sulfur interactions; however, the overall structure of the different bound peptides is anticipated to vary based upon the altered sequences and the binding of the other residues to the particle surface.

Structurally, CD spectroscopy showed significant changes in peptide conformation before and after Pd binding that is strictly dependent on the location of cysteine within the sequence (Figure 3 and Supporting Information, Figure S3). Quantitatively, the largest change in peptide structure was observed with the C6 and C6,11 peptides after Pd binding. Both Pd bound peptides showed a large decrease in ellipticity at ∼203 nm compared to the free peptides, indicative of highly disordered secondary structures (59.3% for C6 and 55.2% for C6,11). This is a result of strong binding to the Pd surface through histidine/cysteine and cysteine/cysteine binding pairs. For the C6A11 and A6C11 peptides on Pd, the peptide structures were substantially less disordered, 35.3% and 26.4%, respectively, because of the presence of only a single binding residue at the six or eleven position. The low extent of unfolding reflects the increased conformational flexibility of the peptides on Pd when anchored at either cysteine residue. For C11 and the original Pd4 peptide, these structures unfolded by 41.0% and 41.4%, respectively, as compared to the analysis of the free peptides in solution.

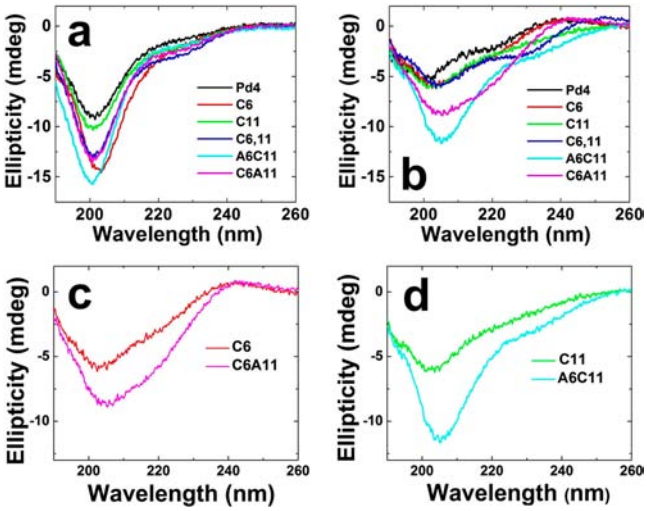

Figure 3. CD analysis of the peptides (a) before and (b) after binding to the Pd nanoparticles. Part (c) presents the CD spectra of C6 and C6A11 peptides bound to Pd, while (d) displays the CD spectra of C11 and A6C11 peptides bound to Pd.

The CD spectra of Pd-bound C6A11 (Figure 3d) showed the presence of a shoulder at ∼240 nm (slightly positive peak) and a wavelength shift from 201 to 205 nm for the dominant negative CD peak. This most likely is indicative of a compact peptide structure on the Pd surface and exhibits partial characteristics of a polyproline type II (PP2) helix (∼18% contribution). This structure assignment is consistent with the spectral features of a 9-mer polyproline peptide (negative peak at 205 nm and slight positive shoulder at 228 nm).[18] The Pd-bound C6 peptide possessed similar CD peaks to C6A11 (Figure 3c), although the C6 bound peptide appears to be less structured and more disordered (59.3%) based on differences in ellipticity. For the set of peptides with cysteine only in the 11 position, the CD spectra of the Pd-bound C11 and A6C11 peptides exhibited similarities in terms of peak shapes and wavelengths, where both represented unordered structures on Pd (Figure 3d). Again, the Pd-bound C11 peptide has a decreased ellipticity relative to A6C11 on Pd and is more unfolded. Lastly, the cysteine double substituted C6,11 adopts a hybrid surface structure on Pd similar to C6 and C11 based on equal ellipticity values and characteristic spectral components of both Pd-bound C6 and C11 peptides. In total, this suggests that the cysteine in the peptide six position likely affects the overall surface structure, while the presence of histidine or alanine at the eleven position attenuates the magnitude of ellipticity, resulting in a less native and more disordered structure. When a cysteine residue was present in the six position, followed by a binding residue at the eleven position, which is observed for the C6 and C6,11 sequences, the peptides adopt a more disordered structure (59.3% and 55.2% on the Pd surface) due to peptide pinning at the central position and additional strong binding at the end of the sequence. It is interesting to note that peptides with cysteine modifications at the same site (C6 and C6A11 vs. C11 and A6C11, Figures 3c and d, respectively) have remarkably similar CD spectra when bound to Pd. More importantly, the particles capped with the peptides from the first group possessed similar catalytic activities, while those capped with peptides from the second group had increased, similar reactivities. Furthermore, the peptide structural differences can also be resolved using computational modeling, where it appears that these subtle conformational differences observed by CD for the peptide set contribute to the large differences in catalytic performance.

To investigate the trends in peptide binding noted using CD studies, the adsorption of the six different sequences on Pd {111} surfaces was investigated using the INTERFACE-CHARMM force field,[17,19,20] including the specifically stronger bonds of the cysteine thiol sulfur to Pd to reflect covalent bonding contributions (see Supporting Information for details).[21] The equilibrium binding conformation of single peptides was flat-on in all cases and surface-bound water was almost fully replaced (Figure 4 and Supporting Information, Figure S4). Attractive sites on the metal surface for the peptides were not the atoms in the top metal layer, but the atoms in the two layers underneath. This epitaxial interaction mechanism, which is well supported by other simulation and experimental studies,[8,17,22−24] leads to the meandering patterns of the peptides that roughly follow the hexagonal symmetry of the {111} surface. The thiol group also showed a preference toward epitaxial sites in agreement with experimental observations on Au surfaces.[25,26] Moreover, the relative trend in computed binding energies of individual peptides to the Pd surface (Supporting Information, Figure S5) agrees with the reported binding constants of Figure 1c. Accordingly, the C6A11 peptide is more strongly bound than the A6C11 peptide even though particles of the same size are produced. The stronger attraction of C6A11 is related to tighter surface contact at the sixth residue next to a sterically demanding proline in the seventh position as opposed to loosening the surface contact by positioning an alanine residue in the sixth position as in A6C11. Local tightening of surface contact appears to be a main

dx.doi.org/10.1021/ja402215t | J. Am. Chem. Soc. 2013, 135, 11048−11054

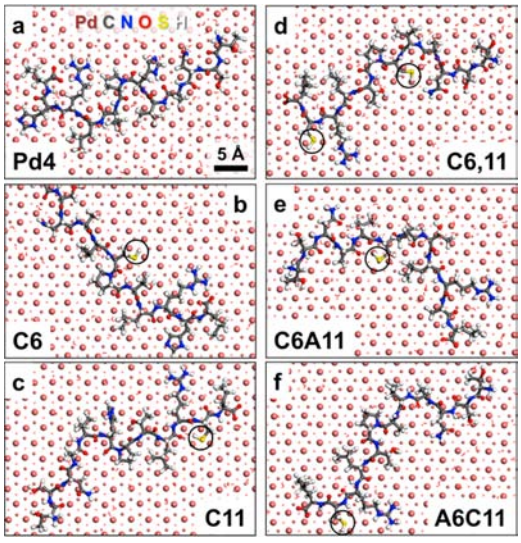

Figure 4. Top view onto equilibrium conformations of single peptides adsorbed on extended Pd {111} surfaces in aqueous solution from MD simulation for (a) Pd4, (b) C6, (c) C11, (d) C6,11, (e) C6A11, and (f) A6C11. The position of partly covalently bound SH groups in cysteine is highlighted. Metal atoms are shown in decreasing size from the top to sublayers.

contributor to stronger adsorption of cysteine-containing peptides versus cysteine-free peptides (Supporting Information, Figure S5 and Figure 1c). The localized attraction of cysteine to one epitaxial site on a facet is also in contrast to stabilization of an area of multiple epitaxial sites by histidine, especially the conformationally flexible histidine in the eleventh position (Figures 4a and b). In agreement with TEM data (Table 1 and Figure 2), histidine appears to be a better growth-limiting residue than cysteine and leads to smaller particle sizes.

It is important to realize that the nanoparticles produced consist of multiple facets[27] and binding measurements by QCM rely on polycrystalline substrates that contain {111}, as well as {100} and {110} surfaces. Moreover, adsorption of peptides may not create perfect monolayers of 0.4 nm thickness.[28,29] Earlier QCM and AFM studies on Au {111} surfaces showed irregular peptide agglomerates that were related to interactions between multiple peptides and potentially biomolecule folding on the surface.[16] The current QCM data similarly show the doubling of surface coverage from lower to higher concentration (Figure 1a and Supporting Information, Figure S1), suggesting increased peptide adsorption at higher concentrations. The Langmuir adsorption parameters including binding constants are averaged over {hkl} facets and multiple peptides, thus potentially reflecting peptide-surface as well as peptide−peptide interactions. It has recently been suggested that the influence of such interactions can diminish adsorption energies from −50 kcal/mol for single peptides to less than −10 kcal/mol for peptides in multilayers.[30] Binding free energies of −8 to −9 kcal/mol from the Langmuir fit reflect possible multilayer formation and correspond to the strength of about 3 hydrogen bonds (Figure 1). The adsorption of the first peptide, including a partly covalent thiol bond, is expected to be higher, possibly −50 to −85 kcal/mol as seen in the simulation (Supporting Information, Figure S5). Furthermore, the long time to reach binding saturation likely arises from peptide surface rearrangement.

As is evident from the CD studies and molecular modeling, different peptide conformations are present on the metallic surface. This effect arises from the position of the cysteine within the overall sequence. To this end, when cysteine is present in the sixth position, the near covalent interaction of the thiol with Pd pins the sequence directly at the center of the biomolecule to the metallic surface. This binding is enhanced by the sterically demanding proline residue at the seven position that has significant effects on peptide secondary structure, thus greatly minimizing the degree of sequence flexibility once bound. This is in contrast with the peptides that position the cysteine residue at the eleven position, which demonstrated increased flexibility when bound to Pd. In this regard, peptide pinning is present at the C-terminal region, allowing the rest of the sequence additional freedom to bind to the metallic surface. Such pinning and flexibility effects were predicted by computational modeling and observed via CD studies that displayed similar peptide structures when bound to the particle surface for the C6 and C6A11 peptides, as well as for the C11 and A6C11 sequences. This degree of flexibility may play a dramatic role over the catalytic activity of the particles, which is dependent upon the exposure of the metallic surface to reagents in solution.

Upon characterization of the particle/peptide surface structure, Stille C−C coupling was used to probe the catalytic activity of the particles (Figure 5). Such studies can be

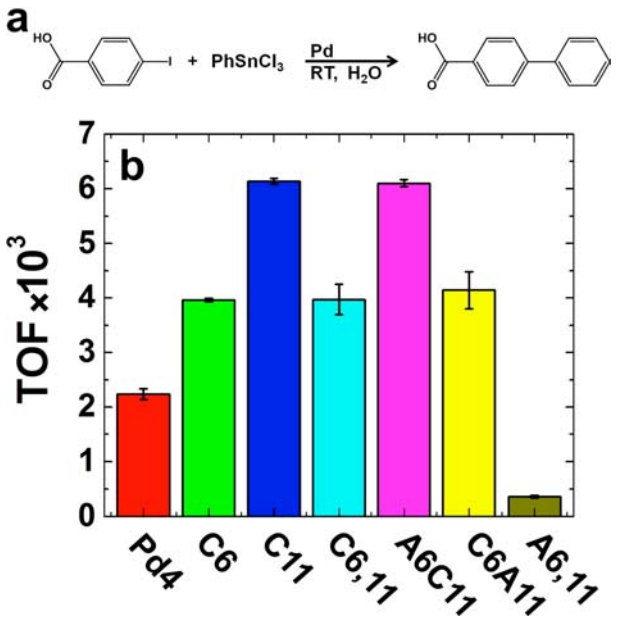

Figure 5. TOF analysis of the peptide-capped Pd nanoparticles for Stille coupling. Part (a) presents the model catalytic reaction, while part (b) displays the TOF values achieved using the nanoparticles capped with the indicated peptide. Pd4 and A6,11 data acquired previously.[12]

employed to ascertain the structural effects of the peptides on the overall material properties. Note that particles of nearly identical sizes were used for this reaction, thus differences in the reactivity are likely attributable to changes in the peptide/particle surface structure. For this reaction, the coupling of 4-iodobenzoic acid with $PhSnCl_3$ to prepare biphenylcarboxylic acid in water at room temperature was used (Figure 5a). From these studies, a clear trend in the catalytic activity was noted that directly depended upon the cysteine position within the

dx.doi.org/10.1021/ja402215t | J. Am. Chem. Soc. 2013, 135, 11048−11054

peptide sequence; however, the reactivity was independent from the global peptide binding strength. Such results were quite surprising as thiols are well-known poisons for noble metal-based nanocatalysts.[31,32] The opposite increase in reactivity could be related to an active role of the thiol groups to support atom leaching, a proposed step in nanoparticle-driven C−C coupling, by stabilizing local defects. Further poisoning effects are likely to be attenuated by the binding of the additional sequence residues to the particle surface, as discussed below.

For comparison, as previously reported, the Pd4-capped particles demonstrated a TOF value of 2234 ± 99 mol product (mol Pd × hr)$^{-1}$.[12] For the particles capped with C6, C6,11, and C6A11 peptides, an approximate 2-fold increase in the reaction efficiency was observed, displaying TOFs of 3963 ± 28 mol product (mol Pd × hr)$^{-1}$, 3974 ± 280 mol product (mol Pd × hr)$^{-1}$, and 4147 ± 340 mol product (mol Pd × hr)$^{-1}$, respectively. Note that for all of these peptides, the strongest residue binding was incorporated at the six position of the sequence. Remarkably, a nearly 3-fold TOF increase over the Pd4-capped particles for the model reaction was observed for the materials prepared using the C11 and A6C11 with TOF values of 6138 ± 55 mol product (mol Pd × hr)$^{-1}$ and 6097 ± 65 mol product (mol Pd × hr)$^{-1}$, respectively. For these sequences, weaker binding was incorporated at the sixth position as compared to the stronger binding of the cysteine residue at the eleventh position. Such high TOF values indicated a direct correlation between the peptide sequence and localized surface binding, particle surface structure (based upon CD and theoretical modeling), and catalytic reactivity. For comparison, the A6,11 peptide, with both histidines replaced with alanines, was previously employed to prepare peptide-capped Pd nanoparticles that demonstrated a TOF value of 361 ± 21 mol product (mol Pd × hr)$^{-1}$.[12] These materials, whose peptide removed thiol-binding residues completely, demonstrated the lowest degree of reactivity, following the anticipated trend, which likely was an effect of the individual residues at specific peptide sequence positions.

Comparing the reactivity of the particles as a function of the cysteine position (Scheme 1) provides important evidence to indicate that the materials functionality can be directly tuned and even enhanced through individual residue changes at the peptide sequence level. Note that the Stille C−C coupling reaction has been suggested to occur via an atom leaching mechanism.[5,33] In this approach, during oxidative addition at the particle surface via the aryl halide, abstraction of Pd is possible. From this, the reaction then occurs in solution, where a free Pd species is released after completion of the reaction. This species can then be recycled through the reaction, providing sufficient starting material is present, or be quenched by the remaining nanoparticles. In the present study, greater TOF values were observed from the particles capped with cysteine-containing peptides over the cysteine-free parent Pd4 sequence. This suggests that such modifications alter the structure/binding of the peptide on the particle surface, consistent with the CD and modeling data, to give rise to this level of reactivity increase. This is surprising in light of known thiol-based poisoning of catalytic particles.[31,32] In general, strong thiol binding at active sites in dispersed Pd catalysts is observed, along with steric crowding at the surface, both of which contribute to diminished reactivity. Such capabilities are likely to be attenuated by the additional functional groups of the peptide sequence binding to the particle. For the peptides, it is likely that the sequences strongly bind through the thiol moiety of the cysteine residue, which binds at the 3-fold interstitial site on the metallic surface to pin the biomolecule to the inorganic material. From this, the additional residues of the peptide are then arranged to provide optimal surface binding, which changes based upon the position of the cysteine within the sequence. This binding mechanism would provide steric bulk to the ligands to prevent additional thiol-based surface poisoning, while allowing substrates access to the catalytic surface to drive Pd leaching during oxidative addition. To this end, these results indicate that thiol-based ligands can be designed as nanoparticle stabilizers for catalytic applications should sufficient offsetting binding moieties be present.

Scheme 1. Effects of peptide sequence on the catalytic activity of peptide-capped Pd nanoparticles

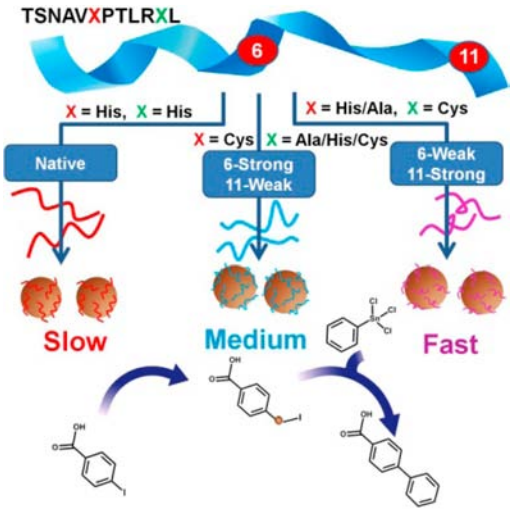

Furthermore, when comparing the modified sequences, an interesting trend was observed; for those peptides with stronger binding at the eleven position and weaker binding at the six position, increased reactivity with greater TOF values was demonstrated (Scheme 1). Such TOFs were larger than those observed for the materials prepared with the sequences that positioned amino acids with stronger and/or equal binding strengths at the six position over the eleven position. In addition, the Pd4-capped Pd nanoparticles, which were the smallest of the set, thus having the greatest surface area, demonstrated the lowest degree of reactivity. Together, this evidence indicates that the peptide sequence and highly localized residue/surface binding inherently affects the particle functionality, controlled via surface binding that can be used as a design point to modify particle properties for applications. To this end, highly localized biomolecular binding, based upon the identity and position of functional groups within the peptide was directly proportional to the catalytic reactivity of the materials. Furthermore, no observable trends were present between the global peptide Pd affinity (ΔG values), the particle size, and the observed reactivity of the materials as nearly the same size nanoparticles were prepared by all five modified sequences. As such, the observed changes in TOF can be attributed to the surface-bound peptide structure, directed via thiol surface pinning based upon the location of cysteine residues within the sequence. These changes in the particle surface morphology, as confirmed by CD and computational

dx.doi.org/10.1021/ja402215t | J. Am. Chem. Soc. 2013, 135, 11048−11054

modeling, are likely to enhance the reaction mechanism, which has been suggested to follow a unique atom leaching process.[5,27,33] For this, changes in the surface bound peptide morphology may more efficiently display the reactive metallic species to the reagents in solution to allow for more rapid Pd leaching during oxidative addition. Should this process be enhanced, additional Pd species would be present in solution to drive the reaction, thus raising the TOF value. Furthermore, increased peptide flexibility on the particle surface was noted for the C11 and A6C11 peptides, as compared to the C6 and C6A11 sequences. This flexibility may also directly modulate the reactivity, where the biomolecules can more readily distort their surface structure to accommodate the interactions of the aryl halide with the metallic surface to facilitate the leaching process. Such peptide structural arguments are supported by the CD observations and modeling studies where similar biomolecular structures were observed for the peptides with cysteine at either the six or eleven position, thus directly correlating with the catalytic observations. As such, localized residue binding affects appear to play a more important role in the activity of peptide-capped materials over the global peptide interaction.

CONCLUSIONS

In summary, we have demonstrated that the properties of peptide-capped nanomaterials can be modulated based upon the position of amino acids within the peptide sequence. In the present catalytic system, we observed an increase in reactivity as a result of cysteine and alanine substitutions at selected sequence positions. From empirical observations, localized peptide modifications were exploited where the placement of such residues within the sequence was determined based upon individual amino acid affinities and computationally predicted motifs. These results indicate that while biocombinatorial techniques can isolate peptides with strong affinity, rational design could be employed to optimize material functionality. Through this, property enhancement was demonstrated with no apparent changes to the metallic core structure. Such capabilities could prove to be useful for a variety of materials outside of catalysis, including plasmonic, magnetic, and electronic structures.

ASSOCIATED CONTENT

Supporting Information

Details of QCM, UV−vis analysis, CD deconvolution, computational methods and results. This material is available free of charge via the Internet at http://pubs.acs.org.

AUTHOR INFORMATION

Corresponding Author

*Corresponding Author knecht@miami.edu; rajesh.naik@wpafb.af.mil

Notes

The authors declare no competing financial interest.

ACKNOWLEDGMENTS

This material is based upon work supported by the National Science Foundation under Grant No. CBET-1157431 (M.K.), DMR-0955071 (H.H.), and by AFRL/RX and AFOSR (H. H. and R.N.). R.C. acknowledges fellowship support from the UM CAS Dissertation Year Fellowship, while N.B. is supported by the National Research Council Research Associateship award. Computational resources from the Ohio Supercomputing Center are also acknowledged.

REFERENCES

(1) Dickerson, M. B.; Sandhage, K. H.; Naik, R. R. *Chem. Rev.* **2008**, *108*, 4935.
(2) Bhandari, R.; Coppage, R.; Knecht, M. R. *Catal. Sci. Technol.* **2012**, *2*, 256.
(3) Briggs, B. D.; Knecht, M. R. *J. Phys. Chem. Lett.* **2012**, *3*, 405.
(4) Chiu, C. Y.; Li, Y. J.; Ruan, L. Y.; Ye, X. C.; Murray, C. B.; Huang, Y. *Nat. Chem.* **2011**, *3*, 393.
(5) Pacardo, D. B.; Slocik, J. M.; Kirk, K. C.; Naik, R. R.; Knecht, M. R. *Nanoscale* **2011**, *3*, 2194.
(6) Mao, C. B.; Solis, D. J.; Reiss, B. D.; Kottmann, S. T.; Sweeney, R. Y.; Hayhurst, A.; Georgiou, G.; Iverson, B.; Belcher, A. M. *Science* **2004**, *303*, 213.
(7) Ahmad, G.; Dickerson, M. B.; Cai, Y.; Jones, S. E.; Ernst, E. M.; Vernon, J. P.; Haluska, M. S.; Fang, Y.; Wang, J.; Subrarnanyarn, G.; Naik, R. R.; Sandhage, K. H. *J. Am. Chem. Soc.* **2008**, *130*, 4.
(8) Coppage, R.; Slocik, J. M.; Briggs, B. D.; Frenkel, A. I.; Heinz, H.; Naik, R. R.; Knecht, M. R. *J. Am. Chem. Soc.* **2011**, *133*, 12346.
(9) Pacardo, D. B.; Sethi, M.; Jones, S. E.; Naik, R. R.; Knecht, M. R. *ACS Nano* **2009**, *3*, 1288.
(10) Pandey, R. B.; Heinz, H.; Feng, J.; Farmer, B. L.; Slocik, J. M.; Drummy, L. F.; Naik, R. R. *Phys. Chem. Chem. Phys.* **2009**, *11*, 1989.
(11) Coppage, R.; Slocik, J. M.; Briggs, B. D.; Frenkel, A. I.; Naik, R. R.; Knecht, M. R. *ACS Nano* **2012**, *6*, 1625.
(12) Coppage, R.; Slocik, J. M.; Sethi, M.; Pacardo, D. B.; Naik, R. R.; Knecht, M. R. *Angew. Chem., Int. Ed.* **2010**, *49*, 3767.
(13) Hoefling, M.; Iori, F.; Corni, S.; Gottschalk, K. E. *Langmuir* **2010**, *26*, 8347.
(14) Chan, W. C.; White, P. D. *Fmoc Solid Phase Peptide Synthesis: A Practical Approach*; Oxford University Press: New York, 2000.
(15) Garcia-Martinez, J. C.; Lezutekong, R.; Crooks, R. M. *J. Am. Chem. Soc.* **2005**, *127*, 5097.
(16) Tamerler, C.; Oren, E. E.; Duman, M.; Venkata-subramanian, E.; Sarikaya, M. *Langmuir* **2006**, *22*, 7712.
(17) Feng, J.; Pandey, R. B.; Berry, R. J.; Farmer, B. L.; Naik, R. R.; Heinz, H. *Soft Matter* **2011**, *7*, 2113.
(18) Rucker, A. L.; Creamer, T. P. *Protein Sci.* **2002**, *11*, 980.
(19) Heinz, H.; Vaia, R. A.; Farmer, B. L.; Naik, R. R. *J. Phys. Chem. C* **2008**, *112*, 17281.
(20) Heinz, H.; Lin, T. J.; Mishra, R. K.; Emami, F. S. *Langmuir* **2013**, *29*, 1754.
(21) Dubois, L. H.; Zegarski, B. R.; Nuzzo, R. G. *J. Am. Chem. Soc.* **1990**, *112*, 570.
(22) Heinz, H.; Farmer, B. L.; Pandey, R. B.; Slocik, J. M.; Patnaik, S. S.; Pachter, R.; Naik, R. R. *J. Am. Chem. Soc.* **2009**, *131*, 9704.
(23) Feng, J.; Slocik, J. M.; Sarikaya, M.; Naik, R. R.; Farmer, B. L.; Heinz, H. *Small* **2012**, *8*, 1049.
(24) Ruan, L. Y.; Ramezani-Dakhel, H.; Chiu, C. Y.; Zhu, E. B.; Li, Y. J.; Heinz, H.; Huang, Y. *Nano Lett.* **2013**, *13*, 840.
(25) Dubois, L. H.; Nuzzo, R. G. *Annu. Rev. Phys. Chem.* **1992**, *43*, 437.
(26) Ulman, A. *Chem. Rev.* **1996**, *96*, 1533.
(27) Ramezani-Dakhel, H.; Mirau, P. A.; Naik, R. R.; Knecht, M. R.; Heinz, H. *Phys. Chem. Chem. Phys.* **2013**, *15*, 5488.
(28) Heinz, H.; Vaia, R. A.; Krishnamoorti, R.; Farmer, B. L. *Chem. Mater.* **2007**, *19*, 59.
(29) Drummy, L. F.; Jones, S. E.; Pandey, R. B.; Farmer, B. L.; Vaia, R. A.; Naik, R. R. *ACS Appl. Mater. Interfaces* **2010**, *2*, 1492.
(30) Ramezani-Dakhel, H.; Ruan, L. Y.; Huang, Y.; Heinz, H. *Submitted* 2013.
(31) Ibanez, F. J.; Zamborini, F. P. *Langmuir* **2006**, *22*, 9789.
(32) Quinn, R.; Dahl, T. A.; Toseland, B. A. *Appl. Catal., A* **2004**, *272*, 61.
(33) Pacardo, D. B.; Knecht, M. R. *Catal. Sci. Technol.* **2013**, *3*, 745.